SES COLLEGE SREEKANDAPURAM

(Accredited by NAAC with 'B' Grade) Affiliated to Kannur University

Criterion 3
Research,Innovation and Extension

3.3- Research Publication and Awards

3.3.2 Number of research papers per teachers in the Journals notified on UGC website during 2020-2021

Physical properties of photo assisted chemically synthesized Cu-doped tin sulphide porous thin films

A. C. Dhanya, K. Deepa & T. L. Remadevi

Springer

Springer

Physical properties of photo assisted chemically synthesized Cu-doped tin sulphide porous thin films

A. C. Dhanya[1] · K. Deepa[2] · T. L. Remadevi[3]

Abstract

Undoped and Cu-doped films exhibited hexagonal SnS_2 structure with different preferred orientations. The doped films cover almost all the surface uniformly with agglomerated bigger crystallites. As prepared films were highly resistive and became conducting on doping. Both films were found to be Sn-rich and the doped films confirmed the presence of copper through EDAX analyzer. There was a considerable redshift in the absorption threshold from the bulk for Cu-doped SnS_2 thin films. All the films were highly reflecting in the infrared region and the reflectivity of the films decreased with doping concentration. Conducting tin sulphide nanostructures are highly applicable in dye sensitized solar cells.

Keywords Conductivity · Tinsulphide · Thin films · Nanostructures · XRD · UV

1 Introduction

Tin sulphide is an interesting potential contender for use as an absorber layer in thin-film solar cells because of its constituent elements, tin and sulphur which are abundant, non-toxic and the optimum direct energy bandgap (1.35 eV) for photovoltaic solar energy conversion. The photovoltaics (PV) area is rapidly growing based on new materials and deposition approaches. At present, PV is predominately based on crystalline and polycrystalline Si and is growing at > 40% per year. Increased cell efficiency and reduced manufacturing expenses are critical in achieving reasonable costs for PV and solar thermal. Presently, both cadmium telluride and CIGS (copper indium gallium selenide) are used as p-type absorber layers, but they are formulated from toxic, scarce constituents [1]. But tin sulphide is formed from cheap, earth-abundant elements, and is non-toxic. It also satisfies the appropriate optical property like high optical absorption coefficient and p-type conductivity required for absorber layer [2]. The theoretical calculation of power conversion efficiency of a tin sulfide-based solar cell as absorber layer expects to be as high as 32%, which is comparable to crystalline silicon and competent enough with that of the currently available CdTe and CuInS2 absorber materials [3, 4].

Tin monosulphide is a promising semiconductor, as it absorbs light within peak solar radiation wavelengths (1.1–1.4 eV) comparable to that of CdTe in the visible range and has a high absorptive coefficient of > 104 cm^{-1}. Tin sulphide thin films also have high photoelectric conversion efficiency. Moreover, the binary compound SnS provides much simpler chemistry than multicomponent $Cu_2ZnSn(Se, S)_4$. From the technological point of view, p-type tin sulphide (SnS), tin disulphide (SnS_2) and the compound Sn_2S_3 can be used as absorber layer in thin-film solar cells. The n-type SnS can be used as window layer in solar cells. They have also an important position in optoelectronic devices and IR detectors working in the IR region due to its high transmittance [5].

Though various physical and chemical deposition techniques have been carried out by many researchers, the development of films with required properties suitable for specific applications by photo-assisted chemically deposition is rare in the literature.

The modification of properties of semiconductors by deliberate doping with suitable dopants is exciting. The role of doping concentration on various properties of

✉ A. C. Dhanya
  acdhanyaac@gmail.com

1 Department of Physics, S.E.S. College Sreekandapuram, Sreekandapuram, Kannur 670631, Kerala, India

2 Department of Physics, P.R.N.S.S. College Mattannur, Mattanur, Kannur 670702, Kerala, India

3 School of Pure and Applied Physics, Kannur University, Kannur, Kerala, India

semiconducting thin films is important from the viewpoints of basic physics as well as applications. In the present work, attempts have been made to improve the optical and electrical properties of photo-assisted chemically deposited tin sulphide films by copper doping.

2 Experimental

2.1 Photo-assisted chemical deposition method (PCD)

The experimental set-up composed of UV lamp of 125 W emitting radiations of 355 nm and reaction bath in quartz vessel with a magnetic stirrer. The amount of UV energy absorbed by the reaction vessel is too small as it is made of quartz. The substrate placed vertically in the reaction solution very near to the UV source and the energy diffuses both into the solution and the substrate. The energy from the UV source is utilized to initiate the molecules of the reaction bath. Selective absorption of photonic energy by the reactant molecules or atoms initiates the process by forming reactive free-radical species that can interact to form a desired film product. The solution was continuously stirred using a magnetic stirrer to avoid the sedimentation on the substrate or at the bottom of the container.

In the case of irradiation of a substrate there may occur photo-induced effect which causes an enhancement of surface migration and re-arrangement of adsorbing atoms. Although there occur both homogeneous and heterogeneous nucleation, due to the slow release of ions by the metal complexes, heterogeneous nucleation leading to uniform nucleation will be high-flying in PCD. The average deposition rate will be lower in PCD than other methods. As a result, the sedimentation on the bottom surface of the quartz beaker will be negligible and after a single deposition, the chemical bath can be re-used for further depositions. The photo-assisted chemical deposition is less intense and slower than that of the thermally activated processes, such as chemical bath deposition (CBD). In PCD, the reaction rate can be easily controlled by adjusting the time of illumination.

Chemical bath contain 1 M $SnCl_2$ dissolved in 10 ml glacial acetic acid followed by the addition of 1 ml hydrochloric acid, 15 ml tri-ethanol amine (TEA), 20 ml ammonia solution and finally 1 M thioacetamide. TEA acts as complexing agent to hold the metal ions.

The deposition was carried out on soda lime glass substrate with a dimension of 7.5×2.5 cm which was cleaned thoroughly by continuous washing in different solutions. Initially, glass substrates were kept in the chromic-sulfuric acid for 24 h. The residues left on the surface were then removed by rinsing the substrate very thoroughly with pure distilled water. The substrates rinsed in distilled water were dried by blowing hot air and used for film deposition.

The doping has been achieved by adding required amount of copper chloride in the cationic solution. The sample preparation was done by adding 0.5, 0.75, and 1.0 wt% of copper chloride along with the cationic precursor. The solution was continuously stirred using a magnetic stirrer at each step of adding up of the precursors to obtain a homogenous solution. The resultant solution was a milky precipitate at first, changed to golden brown and finally to black colour. The deposition was carried out for 3 h on pre-cleaned glass substrates by photo-assisted chemical deposition method. Films were annealed to 100^0C for 15 min. The un-doped and doped samples were named as UD, 0.5 Cu, 0.75 Cu and 1 Cu, respectively.

3 Results and discussion

Variation of thickness of the samples with doping concentration is shown in Fig. 1. The thickness of the film increases with the increasing amount of copper.

4 Structural characterisation

The X-ray diffraction patterns of un-doped and copper-doped thin films synthesized by PCD is shown in Fig. 2. The plot indicates that the un-doped and doped samples have an XRD peak matching with hexagonal structure of SnS_2 [JCPDS Cardno. 89–3198]. In un-doped sample, the peaks are along (100), (004) and (103) planes, while in doped film, it has been changed to (101), (102) and (110) planes.

On 0.5wt% of doping, the film is monocrystalline and preferential orientation changed to (102). As the amount of doping increases, the film becomes polycrystalline and the (101) and (110) peaks evolve with some intensity. With 0.75 wt% of Cu, the predominant orientation of the film remains as (102) direction with improved intensity. The increase in doping concentration increases the intensity of the diffraction peaks up to 0.75 Cu and then decreases. Thus, the optimum amount of doping may be 0.75 Cu to obtain highly crystalline copper-doped thin films. Doping with copper resulted in the formation of some defects in the crystal structures, which in turn changes the intensity of the preferred orientation. At higher doping level, the film shows poor crystallinity. No characteristic peaks of impurity are detected from the XRD analysis.

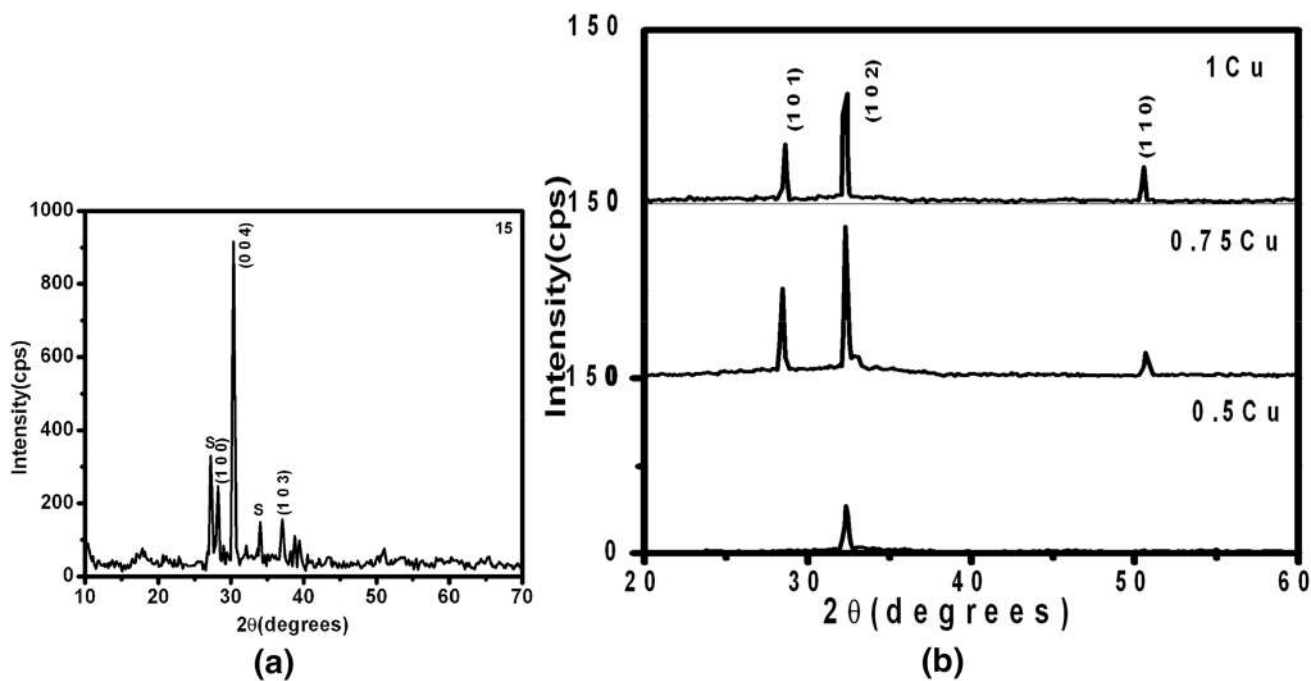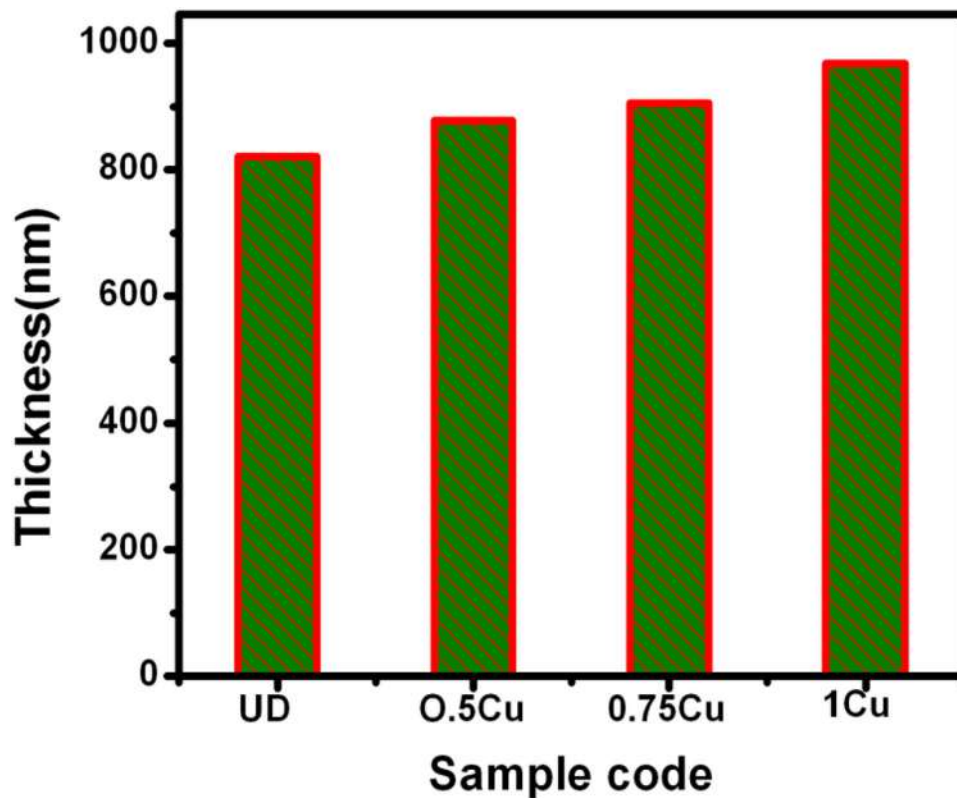**Fig. 1** Thickness of undoped and Cu doped SnS$_2$ films

Fig. 2 X-ray diffractograms of **a** as prepared and **b** Cu doped SnS$_2$ films

The mean crystallite size calculated using the relation (1), improves on doping and the strain calculated using the relation (2) is tensile in nature.

$$D = 0.94\lambda/\beta\cos\theta, \tag{1}$$

$$\varepsilon = \frac{a - a_0}{a_0}. \tag{2}$$

The strain is found to decrease on doping. The maximum strain is observed in un-doped sample, may be due to the presence of sulphur. The observed decrease in strain may be correlated to the decrease in grain boundaries [6]. The variation of grain size and strain of the films is depicted in Fig. 3.

Number of crystallites per unit area is calculated using the relation (3) and is found to decrease with doping concentration. Dislocations are most frequently encountered as defects in thin films. Since nucleation occurs at random sites on the substrate surface, misorientations or misfit displacements of the lattices of nuclei or islands exist. Dislocations are incorporated at the boundary of two islands on coalescence. The dislocation density in un-doped and Cu-doped tin sulphide films is calculated using relation (4) and is found to be less for the doped films. Various structural parameters of the samples are given in Table 1.

$$N = \frac{t}{D^3}, \tag{3}$$

$$\delta = \frac{1}{D^2}. \tag{4}$$

4.1 Optical characterisation

The optical transmittance and absorbance spectra of SnS_2 thin-film samples are shown in Fig. 4. The optical

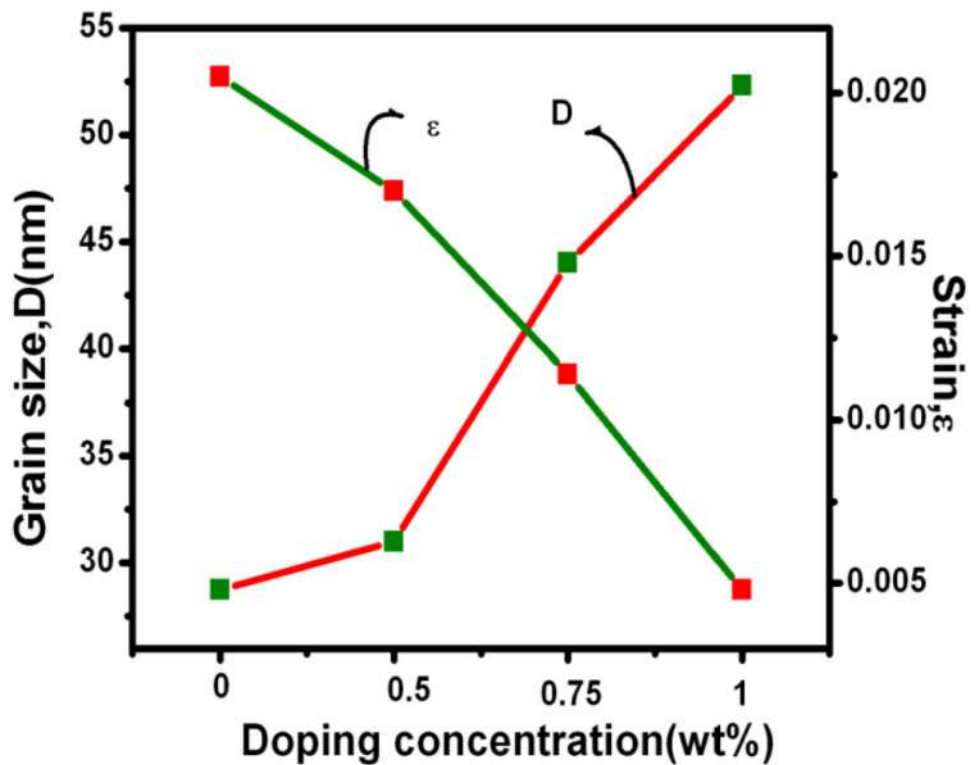**Fig. 3** The variation of grain size and strain of undoped and Cu doped SnS_2 films

Table 1 Structural parameters of undoped and Cu doped SnS_2films

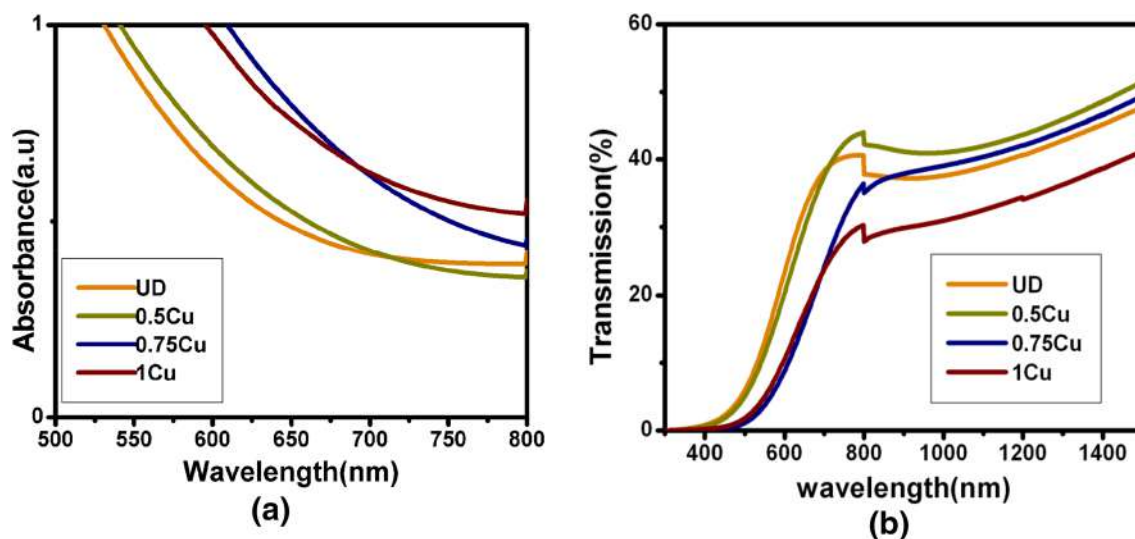| Sample code	Amount of Cu (wt %)	Grain size D (nm)	Strain ε	Number of crystallites $\times 10^{15} (m^{-2})$	Dislocation density $\delta \times 10^{15}/m^2$
UD	0	28.74	0.0205	34.57	1.2
0.5 Cu	0.5	31	0.017	29.48	1.0
0.75 Cu	0.75	44.1	0.0114	10.55	0.52
1 Cu	1	52.3	0.0048	6.77	0.37

Fig. 4 The optical **a** absorbance and **b** transmittance spectra of undoped and Cu doped SnS$_2$films

absorbance indicates a gradual increase from visible to UV region. The increased absorption near band edge is due to the transition of electrons from valence band to conduction band. A considerable red-shift in the absorption threshold from the bulk is observed in Cu-doped SnS$_2$ thin films and may be due to the larger grain size of the doped samples

[7]. Transmission spectra of all the films exhibit a uniform transmittance in the infrared region. In visible region, the samples are non-transparent, indicating maximum absorption in this region.

The band gap energies of the films are determined from the Tauc plot as in Fig. 5 using the relation (5).
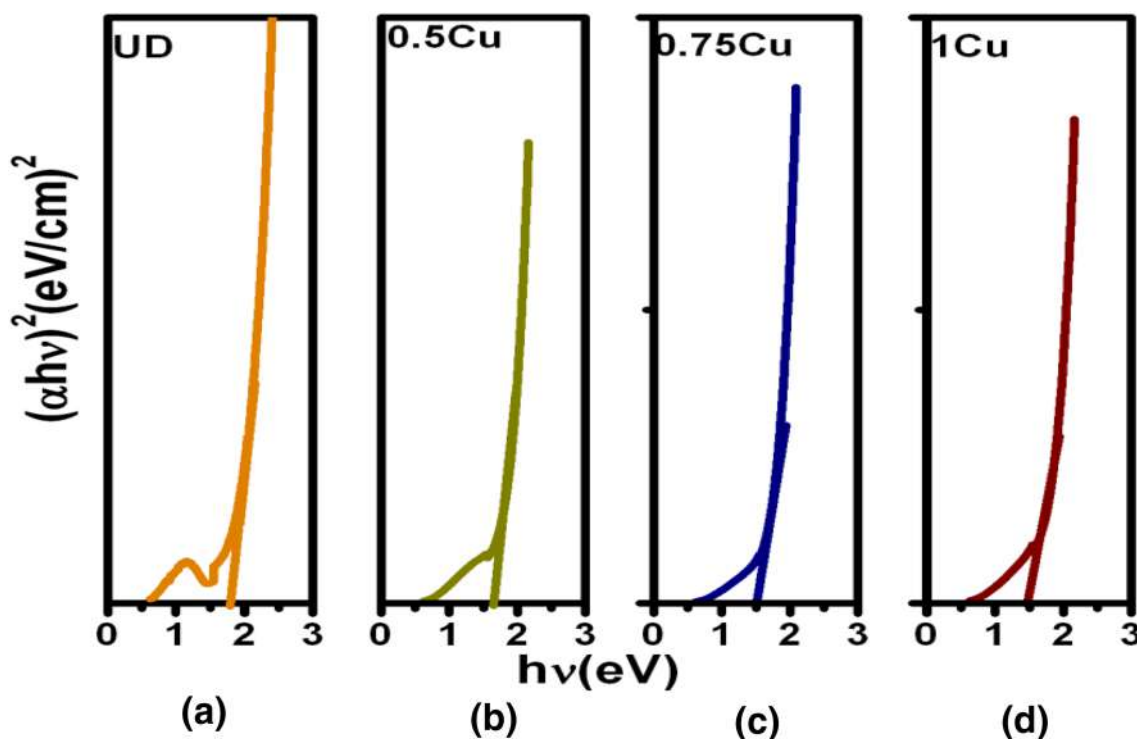

Fig. 5 Tauc plot of undoped (**a**) and Cu doped (**b**–**d**) SnS$_2$ films

Fig. 6 Variation of band gap energy ofundoped and Cu doped SnS_2 films
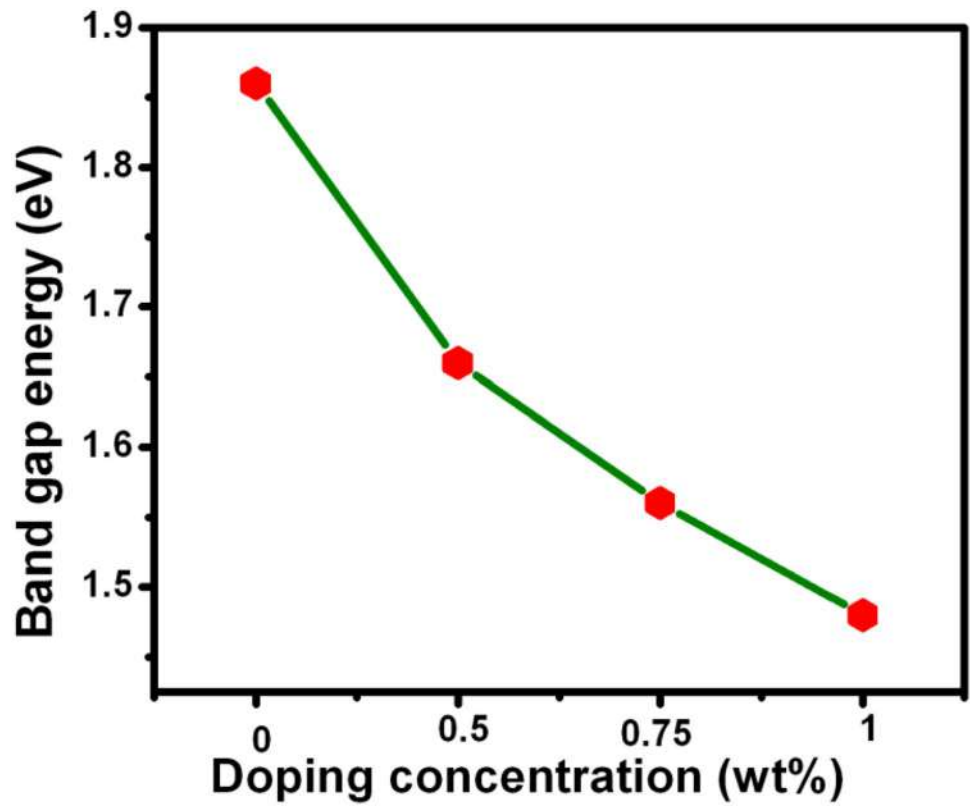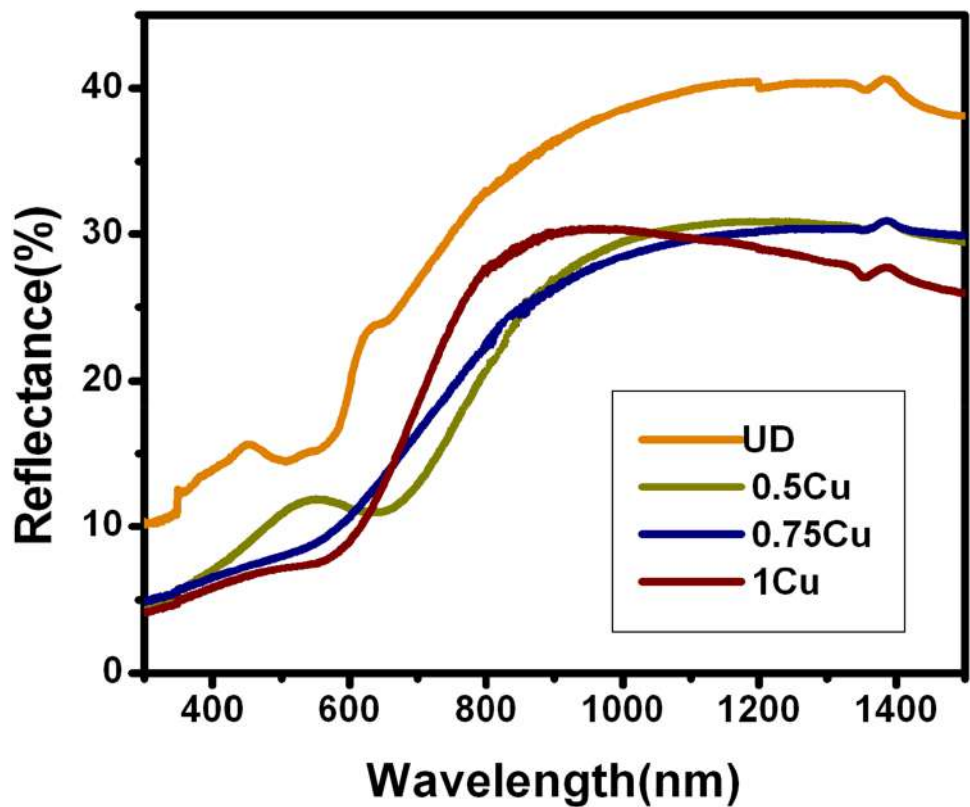

Fig. 7 Reflection spectra of undoped and Cu doped SnS_2films

$$\alpha = \frac{A\left(h\nu - E_g\right)^n}{h\nu}.\tag{5}$$

The decrease in the band gap of Cu-doped SnS_2 films is related to the deformation of the structure. Copper can replace either by substitution or interstitial tin in the tin sulphide lattice creating the structural deformation. Similar results were observed in the study of copper-doped tin sulphide thin films [8]. The values of energy band gap of the films are displayed in Fig. 6.

Reflection spectra of un-doped and doped samples are shown in Fig. 7. All the films are highly reflecting in the infrared region. The reflectivity of the films decreases with doping concentration. This might be due to the lesser number of crystallites in the doped samples [9].
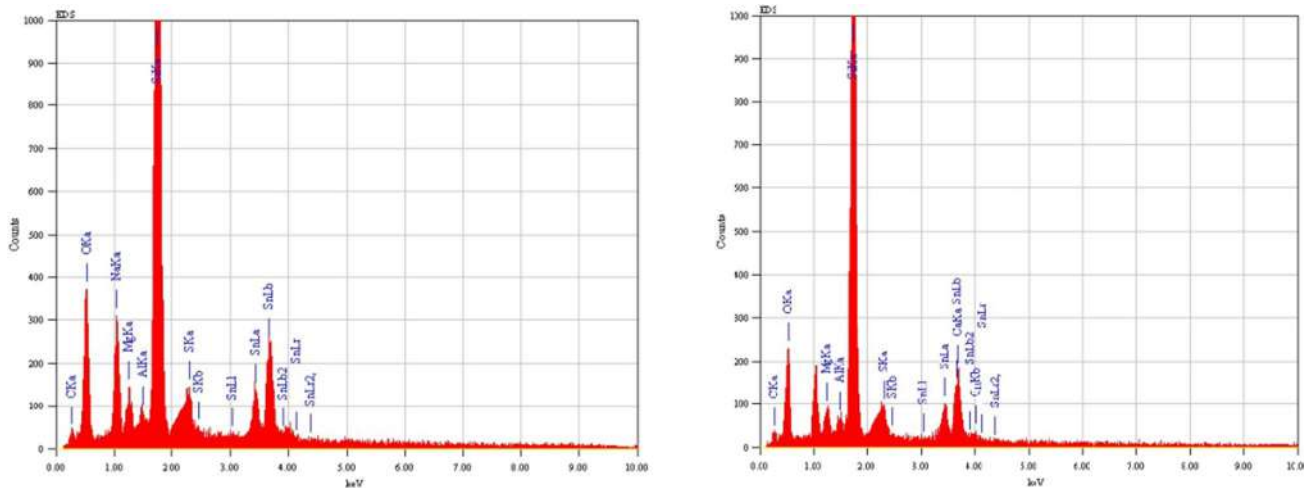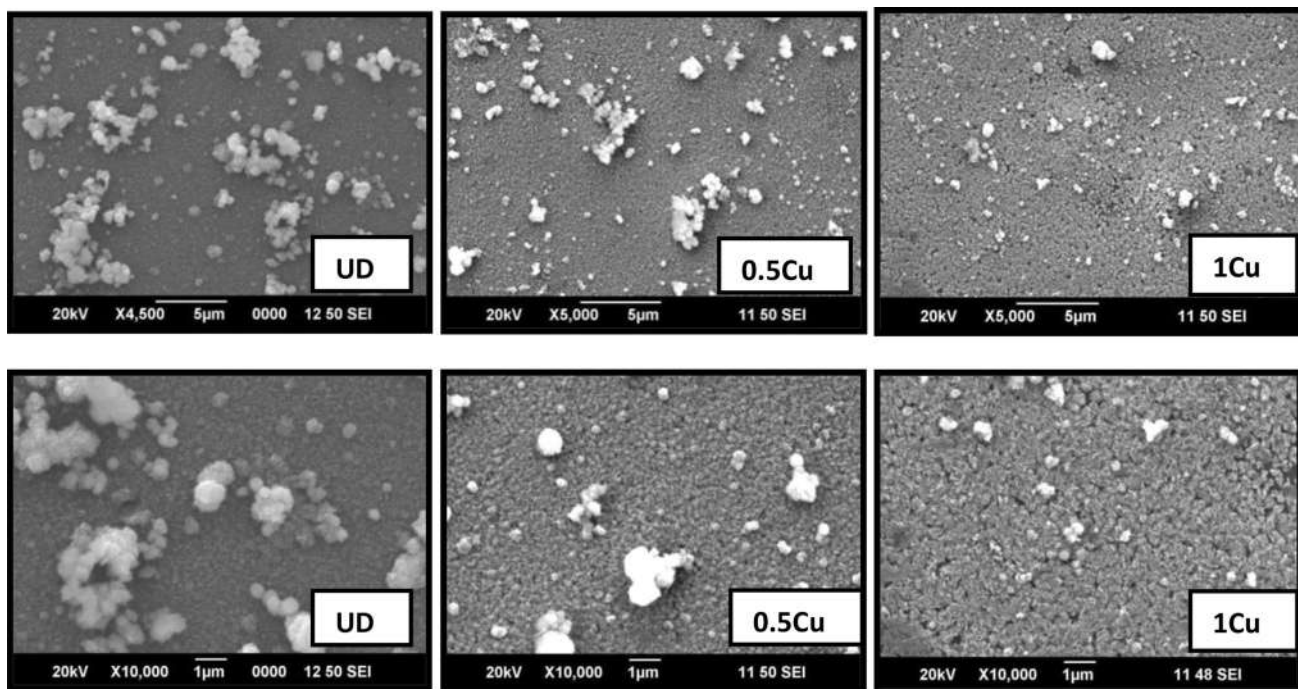

Fig. 8 EDAX spectra of undoped and Cu dopedSnS$_2$ films

Fig. 9 SEM images of undoped and Cu doped SnS$_2$ films at two different magnifications

4.2 Compositional and morphological characterisation

Film composition is determined with the help of an EDAX analyser attached to SEM. Compositions of both un-doped and doped films are shown in Fig. 8. All the films are found to be Sn-rich and the doped film confirms the presence of copper. Figure 9 displays the SEM images of un-doped and doped samples with two different magnifications. Un-doped film contains randomly distributed agglomerated nanoparticles and the doped films contain some pores and appear to be denser.

The surface morphology of the Cu-doped SnS$_2$ films differ from the un-doped one. In the doped films, the surface is uniformly covered with agglomerated crystallites. Some black spots visible in the surface of doped films are due to the pores present in the film which may be formed during deposition. This indicates that the presence of Cu ions in the precursor solution affects the growth of films.

4.3 Electrical characterisation

Un-doped films are highly resistive and become conducting on doping. The conductivity of semiconductors is increased by adding an appropriate amount of suitable impurity or doping. Doping can be done with an impurity which is electron-rich or electron-deficient as compared to the intrinsic semiconductor. When a film is doped with electron-rich impurities, the extra electron becomes delocalized. These delocalized electrons increase the conductivity of doped film due to the negatively charged electron and hence increased the conductivity. Figure 10 represents the room temperature I–V plots of the doped samples. These plots reveal that the conductivity of the samples increases with increase in doping concentration. The presence of surface-stabilized interstitial cations is postulated to explain the occurrence of a surface conduction [10]. The decrease of the electrical resistance of un-doped film might be associated with the deterioration of the film quality. By the insertion of Cu, the surface became smooth. The conductivity computed using Eq. 6 of the samples varies in the range 1.31×10^{-9}–7.26×10^{-9} Ω^{-1} cm^{-1} for the doped samples.

$$\rho = \frac{RA}{L}. \tag{6}$$

Table 2 The room temperature conductivity of Cu doped SnS$_2$ films

Sample name	Conductivity Ω^{-1} cm^{-1}
0.5 Cu	1.31×10^{-9}
0.75 Cu	2.61×10^{-9}
1 Cu	7.26×10^{-9}

Fig. 10 I–V characteristics of Cu doped SnS$_2$ films
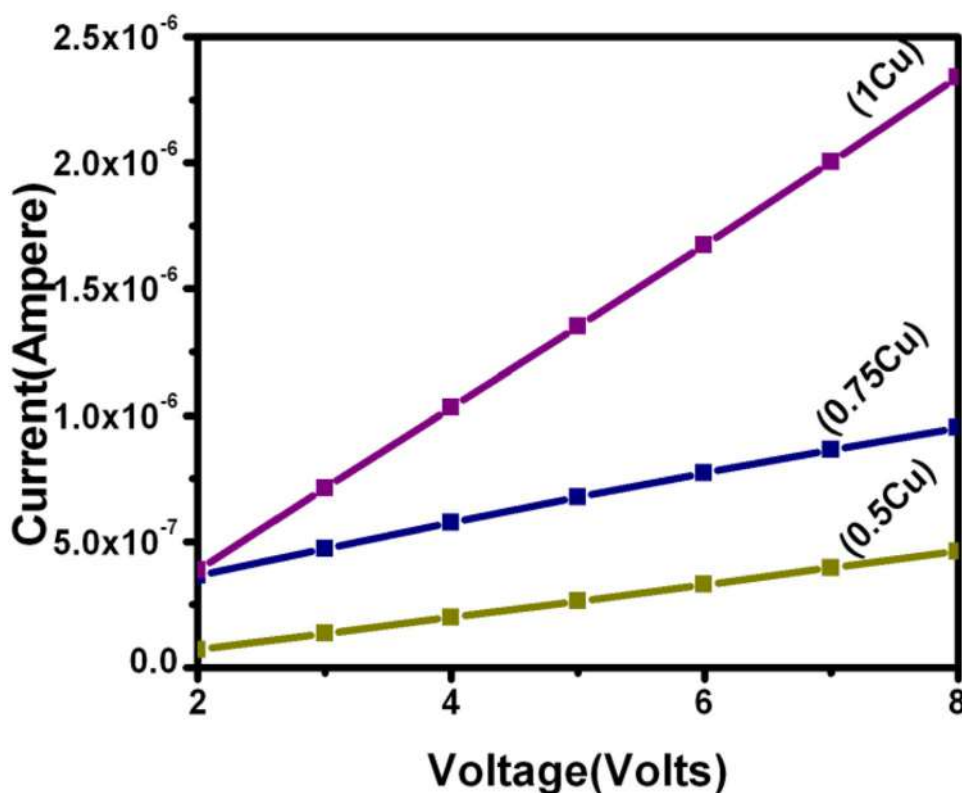
This can be attributed to the increase in film thickness and grain size of the samples. As the amount of copper increases, the film thickness increases which will improve the film continuity. Further, the increase in grain size with thickness results in minimized grain boundaries [11]. As a result, there will be a decrease in carrier scattering and hence an increase in conductivity. The observed values of conductivity of the samples are provided in Table 2.

5 Conclusion

Un-doped and doped films were prepared by photo-assisted chemical deposition method. The doping has been achieved by adding required amount of copper chloride in the cationic solution and the deposition was carried out for 3 h on pre-cleaned glass substrates by photo-assisted chemical deposition method. Un-doped and Cu-doped films exhibited hexagonal SnS_2 structure with different preferred orientations. The thickness of the films increased with copper doping concentration. The crystallite size was improved on doping and the observed strain was tensile in nature. Dislocations which are incorporated at the boundary of two islands were found to be less for the doped films. There was a considerable red-shift in the absorption threshold from the bulk for Cu-doped SnS_2 thin films and, hence the decrease in the band gap.
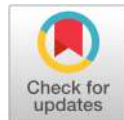
All the films were highly reflecting in the infrared region and the reflectivity of the films decreased with doping concentration. Both films were found to be Sn-rich and the doped films confirmed the presence of copper through EDAX analyzer. The surface morphology of the Cu-doped SnS_2 films differed from the un-doped one. The doped films cover almost all the surface uniformly with agglomerated bigger crystallites. As prepared films were highly resistive and became conducting on doping, the conductivity of the samples varied in the range 1.31×10^{-9}–7.26×10^{-9} $\Omega^{-1}\,cm^{-1}$.

References

1. D. Ginley, M.A. Green, Mat. Res. Bull. **33**(4), 355 (2008)
2. A.J. Andrade-Arvizu, M. Courel-Piedrahita, O.J. Vigil-Galán, Mater. Sci Mater. Electron. **26**(7), 4541 (2015)
3. P.K. Nair, A.R. Garcia-Angelmo, M.T.S. Nair, Phys. Status Solidi A **213**(1), 170 (2016)
4. A. Akkari, C. Guasch, N. Kamoun-Turki, J. Alloy. Compd. **490**, 180 (2010)
5. V.G. Pol, S.V. Pol, A. Gedanken, Langmuir **24**, 5135 (2008)
6. P.P. Hankare, A.V. Jadhav et al., J. Alloy. Compd. **463**, 581 (2008)
7. S. Sur, Z. Ozturk, M. Oztas, M. Bedir, Phys. Scr. **82**, 045604 (2010)
8. N. Sato, M. Ichimura, E. Arai, Y. Yamazaki, Sol. Energy Mater. Sol. Cells. **85**(2), 153 (2005)
9. M. Gunasekaran, R. Gopalakrishnan, P. Ramasamy, Mater. Lett. **58**, 67 (2004)
10. Y. Jiang, W. Sun, B. Xu, M. Yan, N. Bahlawaneb, Phys. Chem. Chem. Phys. **13**, 5760 (2011)
11. A. Goswamy, *Thin film fundamentals*, 1st edn. (New age international Publishers, NewDelhi, 2003)

ChemPhysChem

Accepted Article

This manuscript has been accepted after peer review and appears as an
Accepted Article online prior to editing, proofing, and formal publication
of the final Version of Record (VoR). This work is currently citable by
using the Digital Object Identifier (DOI) given below. The VoR will be
published online in Early View as soon as possible and may be different
to this Accepted Article as a result of editing. Readers should obtain
the VoR from the journal website shown below when it is published
to ensure accuracy of information. The authors are responsible for the
content of this Accepted Article.

WILEY-VCH

Butterfly Methanes: Designing a Novel Class of anti-van't Hoff Carbons

M. J. Saumya[ab#], K. R. Raghi[ab#], D. R. Sherin[b], K. R Haridas[a] and T. K. Manojkumar*[ab]

[a]School of Chemical Sciences, Kannur University, Payyanur Campus, Edat P.O, Kannur-670327, Kerala, India.

[b]Indian Institute of Information Technology and Management-Kerala, Technopark Campus Trivandrum- 695581, Kerala, India

*Corresponding author's e-mail: manojtk@iiitmk.ac.in

(#Both authors contributed equally to this manuscript)

Among different possible non-classical structures, the stabilization of half-planar tetracoordinate carbon conformation is believed to be the most difficult one. In this MS we designed three types of half-planar tetracoordinate carbon compounds computationally by employing hybrid stabilization effects of substituents. The axial hydrogens of unstable half-planar methane are substituted with π-acceptor and σ-donor substituents such as –BH$_2$, –Li and the equatorial substituents selected are a combination of electropositive atoms (σ-donors)/electronegative atoms (σ-acceptors and π-donors). To find out the stabilization factors, we conducted a detailed study on vibrational frequency analysis, molecular orbital analysis (including Natural Bond Orbitals) and electrostatic potential (ESP) analysis of optimized molecular geometries using density functional theory.

Keywords: Non-classical carbon, half-planar methane, butterfly carbon, DFT

Graphical Abstract
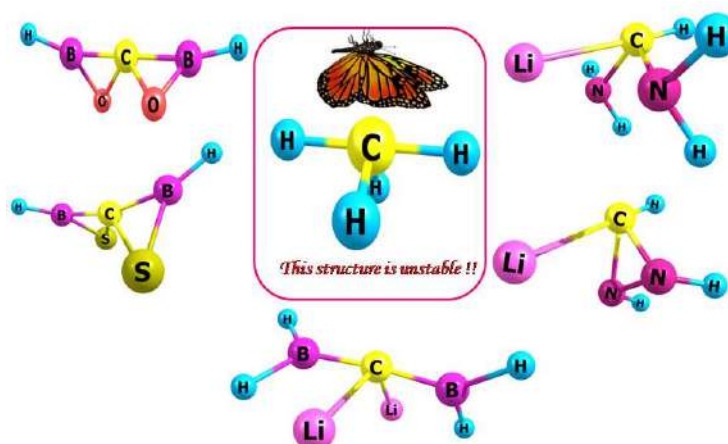
Introduction

The search for novel organic structures has paved the way for non-classical organic compounds that do not adhere to the dogma of tetravalency and tetrahedral geometry of carbon. These kinds of unusual structures may have tetracoordinate or a hypercoordinate carbon centre. The possible conformations for tetracoordinate non-classical carbons are planar, pyramidal, butterfly and umbrella structures[1]. This kind of conformations does have properties distinct from that of the regular tetrahedral geometry. Recent days witnessed multiple reports about the successful synthesis of non-classical carbons. This paper focuses on the stabilization of one of the most exciting non-classical structures known as half planar or butterfly-type carbon compounds. There are only a few reports in the literature about the stabilization of these kinds of structures.
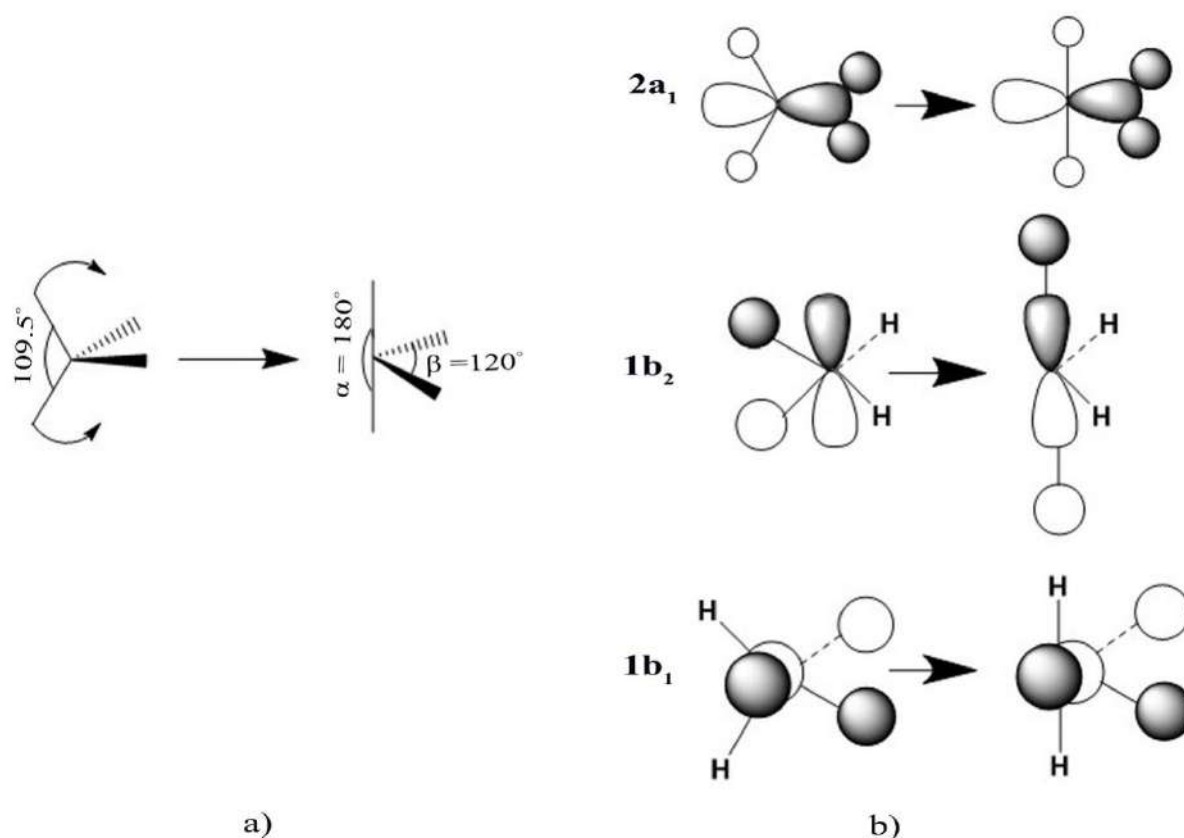
Figure 1.a) Deformation of methane from tetrahedral to half-planar configuration b) Walsh diagram showing the transformation of methane from tetrahedral to half planar geometry[1].

The half-planar (Hp) methane (C_{2v}) can be obtained by twisting the H-C-H angle of tetrahedral (Td) methane from 109.5° to $\alpha = 180°$ and $\beta = 120°$ (Figure 1a). Radius et al.[1] computed energies of both Hp and Td methane and found that Hp is destabilized by 70.56

2

kcal/mol compared with Td conformer. Molecular orbitals (MOs) of Hp type carbon are shown in Figure 1b. The MO's confirm that the instability of the structure can be accounted by the electron-deficient bonding orbitals and electron-rich non-bonding type orbitals. The Walsh diagram in Figure 1b shows that in Hp methane, the p_y (1b$_2$) of carbon gains bonding overlap while the p_x (1b$_1$) remains almost unaffected. The energy of p_z (2a$_1$) increases as it is directed towards the empty coordination site, but from Figure 1b it is clear 2a$_1$ is not a pure lone pair. That is, the localization of the electrons on HOMO creates deficiency of electrons in the σ-bonding plane resulting in the non-availability of electrons for bonding and the destabilization of the Hp carbon configuration. According to Radius and co-workers, if the substituents which can act as σ-donor and/or π-acceptor in axial position and introduction of an external σ-acceptor group (a fifth ligand) which can interact with the higher energy 2a$_1$ (p$_z$) orbital, could substantially narrow the energy gap between the Td and Hp configurations.

These unusual Hp carbon configurations were observed in several carbide clusters like [Fe$_4$C(CO)$_{13}$], the central carbon atom in this molecule is bound to butterfly arrangement of four Fe atoms (Fe$_4$ cluster), and each Fe is connected to three-terminal carbonyls[2-4]. Another class of compounds exhibiting Hp configuration of carbon are rare earth metal complex of yttrium [(Me$_3$SiCH$_2$)Y[(μ-CH2)$_2$SiMe$_2$][(μ-OCMe$_3$)Li(THF)$_2$]$_2$][5] and samarium [(Me$_3$SiCH$_2$)Sm[(μ-OPh)(μ-CH$_2$SiMe$_3$)Li(THF)][(μ-OPh)$_2$Li(THF)]][6]. In these complexes, a methylene carbon or alkyl group is bridging a binuclear metal centre (3c-2e bond) with lithium counter ions in the carbon ligand sphere. In 1995, researchers have synthesized a zirconium complex (Cp$_2$Zr[CH$_2$(HB{C$_6$F$_5$}$_2$)$_2$]), which is the first mononuclear organometallic compound having a pentacoordinate carbon atom, in which the –CH$_2$ carbon is in the Hp conformation[7]. In 1996, Radius et al.[1] have done a detailed theoretical study of a series of zirconium complexes and explored the effect of substituents, X (–H, –CH$_3$,–OH, –CN, –BH$_3^-$) for axial hydrogens in the Hp methane. The results showed that the substitution of two axial hydrogen atoms by –BH$_3^-$ reduces the energy barrier for the deformation from Td to the Hp structure.

The distorted geometry of the carbon atom in the butterfly conformation attracted the attention of several theoretical research groups. In 1996, Wiberg's group theoretically predicted hypothetical tricyclo[2.1.0.0]hexane with a butterfly carbon[8,9] and the same molecule was explored later in detail by Dodziuk's group[10]. In 2003, Minyaev's team conducted studies on carbon polyprismanes, a family of strained cage compounds in which the edge carbon atoms exhibit Hp conformation[11]. Recently, Katin et al. have done a molecular dynamics study on

the thermal stability of [*n*,5] prismanes (*n* = 2-4) and have reported that at cryogenic temperatures, the lifetime of [*n*,5] prismanes significantly increases. This shows the possibility of the experimental observation of this non-classical structures[12]. These reports show that these may be an experimental realization of stabilizing the Hp tetracoordinate carbon compounds. Due to this fact, both theoretical and experimental research in this area has got a greater momentum.

Schleyer's group reported planar tetracoordinate carbon compounds employing two lithium atoms and two nitrogen/oxygen atoms, which revealed the role of these substituents in the stabilization of non-classical carbon configurations by a hybrid effect. A combination of electronegative nitrogen/oxygen atoms and electropositive lithium atoms as substituents produced stable planar tetracoordinate carbon compounds[13]. This manuscript presents the computational design of three types of novel Hp tetracoordinate carbon compounds, type **1-3**. Here, the axial hydrogen/hydrogens of Hp methane are substituted by π-acceptor and σ-donor groups such as –BH$_2$ or –Li. The equatorial substituents are carefully selected in such a way that they are electropositive atoms having σ-donating properties or electronegative atoms which can act as σ-acceptor and π-donors at the same time[14-18]. The structures were confirmed as minima by frequency computations. We carried out MO analysis, natural bond orbital (NBO) analysis and ESP analysis for exploring the bonding properties of these Hp configurations.

Computational methods

All computations were done using the Gaussian 09 program suite[19] using B3LYP functional/6-311++G** basis set. Wave function stability checks were executed at the same level of theory. We further performed the geometric optimization and vibrational analysis at the CCSD/6-311++G** level of theory. Density functional theory and Coupled Cluster theory reported to be highly effective for computing properties of non-classical structures [13,20]. Inclusion of diffused and polarized functions is necessary for computing non-classical structures with highly unusual molecular orbitals. The molecular structures and molecular orbitals were visualized using the ChemCraft software [21]. The NBO analysis[22,23] were performed at the B3LYP/sdd level to gain insights about the electronic structure of compounds. The quantitative analysis of the electrostatic potential on the van der Waals surface was performed at the default settings of the Multiwfn programme package[24] and manifested by the VMD programme[25].

4

Results and discussion

The optimized geometries of type **1-3** compounds are given in Figure 2. Type **1** and type **2** compounds with B-C-B axial bonds are differentiated by their equatorial substituents. In type **1**, the equatorial ligands are electropositive lithium atoms whereas in type **2**, they are the electronegative oxygen/sulphur atoms forming a 3-membered ring. In the case of type **3** compounds, the axial positions are occupied by lithium and hydrogen instead of boron. In **3a**, the equatorial substituents are free –NH$_2$ groups whereas in **3b** they are connected to form a C-N-N ring. The stability of the wave functions was tested. The frequency computations at B3LYP/6-311++G** and CCSD/6-311++G** level of theory showed that these non-classical structures are minima on the potential energy surface (Table S2). The important bond parameters of the obtained structures are given in Table 1. Except **2b**, all the structures show axial X-C-X angle (α) closer to 180° and for **3b**, the equatorial angle Y-C-Y (β) shows a significant deviation from classical geometry. The bond lengths of all the compounds are within the acceptable limits and also in the range of earlier theoretical studies[26-38]. The shorter C-B bond lengths than the typical C-B single bond (1.554 Å) in CH$_3$-BH$_2$ indicate the π-back donation from Cp$_z$ to the empty p-orbitals of boron [39].
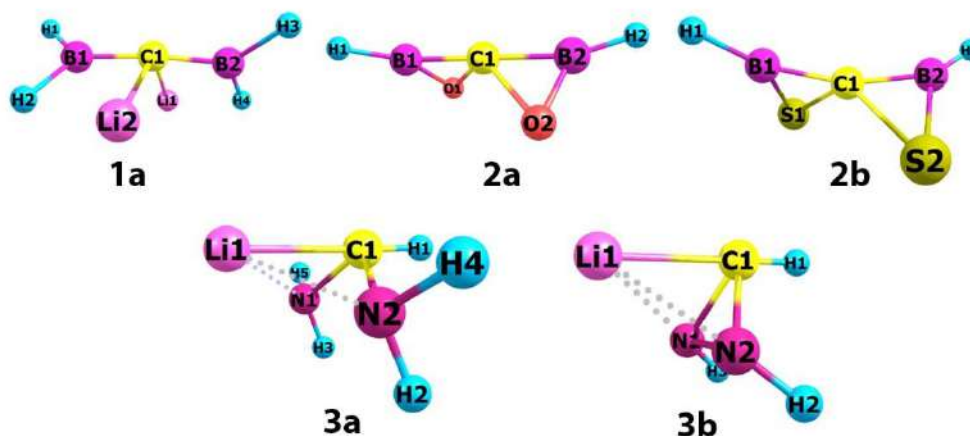

Figure 2. Optimized geometries of type **1-3** compounds at B3LYP/6-311++G** level of theory.

Table 1. The important geometrical parameters computed at the B3LYP/6-311++G** level of theory.

Structural Parameters	Structures				
	1a X1=X2=B Y=Li	**2a** X1=X2=B Y=O	**2b** X1=X2=B Y=S	**3a** X1=Li;X2=H Y=N	**3b** X1=Li;X2=H Y=N
Xi-C (bond length) (i = 1,2)	1.441	1.496	1.494	1: 1.893 2: 1.096	1: 1.915 2: 1.093
C-Y(bond length)	1.937	1.507	1.934	1.501	1.506
X-Y(bond length)	-	-	-	1.956	1.937
α (degree)	174.1	179.9	162.7	178.8	179.2
β(degree)	120.0	115.5	125.4	102.6	59.6

X1, X2, Y & Alpha and beta are shown in Figure 1.

We computed vibrational modes of different structures at the B3LYP/6-311++G** level of theory (Table 2). The C-B and C-Li vibrations of CH_3BH_2 and CH_3Li, computed at the same level of theory, are used as the references. The C-B symmetric stretching vibrational frequency of CH_3BH_2 computed to be 950 cm^{-1} and C-Li symmetric stretching vibrational frequency of CH_3Li is 612 cm^{-1}. The computed C-B symmetric stretching frequencies of **1a** and **2b** are 928 and 930 cm^{-1} respectively. This is slightly smaller than the vibrational mode of the reference compound. The C-B asymmetric stretching vibrations are observed at 1588, 1513 and 1371 cm^{-1} for **1a, 2a** and **2b** respectively. This lowering of frequency in **2b** is due to the bonding of boron to the sulphur atom. It is observed that all the C-Li vibrations in **1a** are coupled with B-H bending modes. The C-Li symmetric stretching vibration observed at 573 cm^{-1} is closer to that of the reference compound. The compound **2a** shows a characteristic deformation of carbon towards pyramidalization at 607 cm^{-1}. It also shows B-O symmetric and asymmetric stretching vibrations at 1195 and 1329 cm^{-1}.

Table 2. The computed vibrational frequencies obtained at the B3LYP/6-311++G** level of theory.

6

Conformations	Vibrational frequencies (in cm⁻¹)				
	C-X Stretching	C-Y Stretching	C-Y bending	X-Y Stretching	Deformation Of C
1a X=B Y=Li	928(S) 1558(A)	573(S) 644(A)	466(T) 514(W)		
2a X=B Y=O	1513(A)	507(A)	403(W)	1329(S) 1195(A)	607
2b X=B Y= S	930(S) 1371(A)				405
3a X1=Li X2=H Y=NH2	X1: 634 X2: 2919		X2: 914 & 1078 (LO) X2: 958 & 1286(LA)		800
3b X1=Li X2=H Y=-N	X1:630 X2: 2923	634(S) 1054(A)	X2:1081(LA) X2: 1136 & 1243 (LO)		694

X1, X2 and Y are shown in Figure 1. S= Symmetric, A = Asymmetric, W = Wagging,
T=Twisting, LA= Latitudinal bending, LO= Longitudinal bending.

* = Y-C-Y bending

† = X1-C-X2 bending

The compounds **3a** and **3b** have C-Li stretching vibrations at 634 and 630 cm⁻¹, which is nearer to that of CH₃Li. The pyramidalization tendencies of the central carbon in **3a** and **3b** are indicated by the bending vibrational frequencies at 800 and 694 cm⁻¹. However, the lower frequency in the case of **3b** is due to the restricted movement of the carbon in the C-N-N ring. The compound **3b** is having C-N symmetric and asymmetric stretching at 634 and 1054 cm⁻¹. C-H longitudinal and latitudinal bending vibrations of **3a** and **3b** given in Table 2 are found to be coupled with N-H vibrations.

The analysis of the MOs (Figure 3 & S1) and NBOs (Table 3& S3) has given a lucid picture of the electronic structure of the designed compounds and its stabilizing factors. These are explained for each of the three types in the following sections.
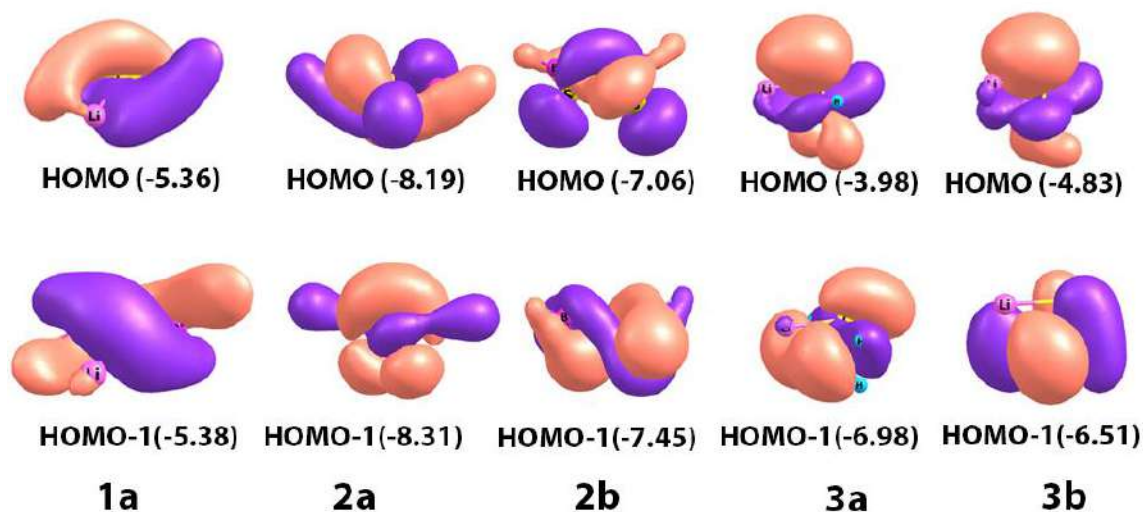
HOMO (-5.36)   HOMO (-8.19)   HOMO (-7.06)   HOMO (-3.98)   HOMO (-4.83)

HOMO-1(-5.38) HOMO-1(-8.31) HOMO-1(-7.45) HOMO-1(-6.98) HOMO-1(-6.51)

1a   **2a**   **2b**   **3a**   **3b**

Figure 3. Plots of HOMO and HOMO-1 of the optimized geometries of type **1-3** (MO energy is given in eV).

Table 3. Summary of the HOMO-LUMO gap and natural charge of the designed compounds.

Property	Conformations				
	1a X = B Y=Li	**2a** X = B Y=O	**2b** X = B Y=S	**3a** X =Li &H Y = -NH$_2$	**3b** X=Li & H Y=-NH
HOMO-LUMO Gap (eV)	4.12	6.70	4.48	3.28	4.13
Natural Charge on C	-1.18	-0.03	-0.72	-0.29	-0.34
Natural Charge on atom X	-0.06	+0.70	+0.39	+0.71(Li) +0.14(H)	+0.75(Li) +0.14(H)
Natural Charge on atom Y	+0.83	-0.62	+0.01	-1.01	-0.64

The MO analysis for **1a** shows the nearly perpendicular orientation of the –BH$_2$ ligands towards each other, which enhances the simultaneous interaction of both the ligand group orbitals with central carbon[40]. The HOMO is a delocalized MO, which represents the back donation from the Cp$_z$ orbital to the empty p orbitals of adjacent boron atoms, thus delocalizing the extra electron density on Cp$_z$. The HOMO-1 looks like a delocalized orbital involving a σ-

8

donation between π-type ligand orbitals and Cp_x[41]. HOMO and HOMO-1 are degenerate orbitals in which the $-BH_2$ MOs involved in the stabilzation of Hp carbon by simultaneously acting as π-acceptors and σ-donors. The NBO analysis predicts the atomic orbital populations of valence p-orbitals as $2p_x^{1.4} 2p_y^{1.4} 2p_z^{1.2}$ which supports the delocalization of electron density from Cp_z and σ-donation of $-BH_2$ groups to the σ-bonding plane. The high Wiberg bond index for C-B bonds (1.67) reconfirm the same. The equatorial lithium atoms with its σ-donating property are acting here as counter ions, which is supported by the representative atomic charges +0.83 on Li, -1.18 on the central C and -0.06 on B. The low Wiberg index (C-Li = 0.13) also shows that lithium acts as a counter ion though the C-Li bond (C-Li bond length is 1.937 Å). There exists an electrostatic attraction between lithium atoms and adjacent hydrogens of $-BH_2$, which is clear from the fact that the bond length of B1-H2(or B2-H4) is 1.25 Å while that of B1-H1 (or B2-H3) is slightly lower and is 1.20 Å. The charge on H2 (or H4) computed to be -0.14 and that on H1 (or H3) is -0.04 further confirms the electronic interaction. For a better understanding of the intermolecular interactions stabilizing the compounds, the inspection of the ESP maps on the van der Waals surface of the compound was done. This shows carbon and $-BH_2$ ligands in a pool of negative potential region represented in red colour and lithium atoms in the positive potential region represented in blue shade with surface maxima as 170 kcal/mol (Figure4a).

The type **2** compounds have got divalent oxygen/sulphur atoms as equatorial ligands and forms 3-membered ring with the axial borons. The balance between electron delocalization from Cp_z of central carbon to the p-orbital of boron atoms and inductive stabilization by the σ-accepting nature of electronegative equatorial substituents stabilizes the compounds. Rather than the inductive stabilization, the lone pair electrons of oxygen atoms have a negative hyperconjugation like effect where the electron density is transferred from a filled π- or p-orbital to the neighbouring orbital of carbon. That is, the oxygen atoms together with boron atoms produce an effect similar to that of captodative stabilization. Here, the donor atom supports the interaction of Cp_z with acceptor orbitals. This is exactly observed in the HOMO-1 of **2a**, where the oxygen lone pair orbital interacts with Cp_z, pushing the electron density to empty p-orbital of boron. This stabilization could effectively stabilize the extra electron density on Cp_z orbital. The butterfly configuration of type **2** molecules supports interaction of orbitals on oxygen and sulphur with that of carbon and boron atoms. The HOMO of **2a** shows simultaneous interaction of Cp_y, ligand group orbital of $-BH_2$ and oxygen lone pair orbital of the 3-membered ring, while HOMO-1 in **2b** shows a similar interaction. From the energy

9

values, it is clear that substituting with divalent equatorial substituents could lower the energies of MOs when compared to that of type **1** compounds. But it distorts the Hp geometry in **2b** with α=162.7° In addition, the charge distribution in **2a** [charge on H1 (or H2) = -0.07, charge on B1 (or B2) = 0.70, charge on central C atom = -0.03, charge on oxygen atoms = -0.62] shows the effective balance as the carbon has less negative charge. This is further substantiated by the analysis of ESP plots (Figure 4b). It shows oxygen/sulphur atoms lying in the negative potential region, boron and hydrogen atoms in the positive potential region and central carbon in an intermediate potential region. Further, the valence orbital population $2p_x^{0.9} 2p_y^{1.0} 2p_z^{0.9}$ of central carbon indicates the effective delocalization of Cp_z electrons. The Wiberg indices C-B = 0.91, C-O = 0.85 and O-B = 1.09 support the bonding in C-O-B ring, which enhances the Hp configuration of carbon.
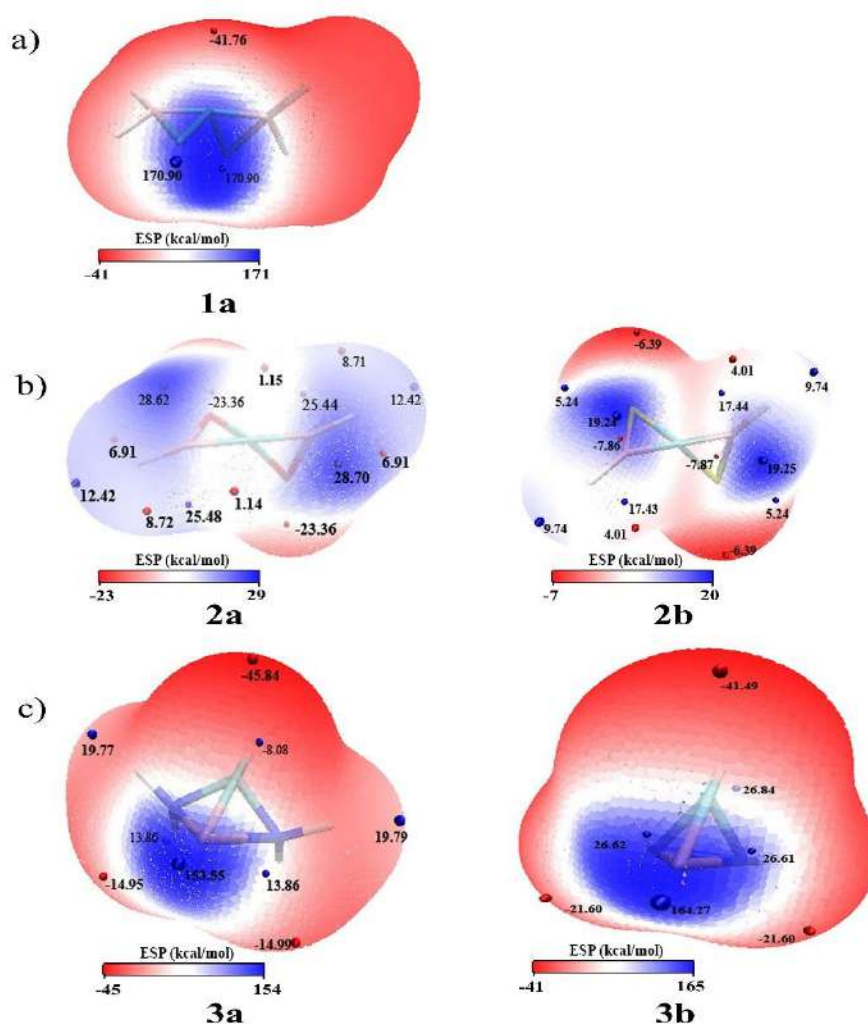

Figure 4. Plots of ESP on the van der Waals surface of the designed Hp compounds at the B3LYP/6-311++G** level of theory. Blue indicates positive and red indicates negative potential. Surface

10

local minima and maxima of ESP (expressed in kcal/mol) are represented as red and blue spheres respectively.

In type **3** compounds, we have hydrogen and lithium atoms as axial ligands with σ-accepting $-NH_2$ ligands as the equatorial substituents. Here, the repulsion by the lone pair electrons is turned off by their spatial orientation inclined towards the electropositive lithium atom. The strong bridging tendency of lithium to heteroatoms as well as its strong electron-donating ability together with inductive stabilization and the negative hyperconjugation like effect of the $-NH_2$ are playing significant roles in the stabilization. The lithium atom forms ionic bonding with carbon (Wiberg index of C-Li = 0.25, charge on Li atom = +0.7) in both the compounds, thereby acting as a good σ-donor and stabilizing the excess electron density in HOMO by electrostatic attraction (Figure 4c). In HOMO, the interaction of lone pair electrons of nitrogen with Cp_z orbital of carbon promotes the transfer of its electron density towards the electropositive lithium atom. The HOMO-1 is stabilized by the negative hyperconjugation effect of lone pairs of nitrogen to the electron-deficient σ-bonding plane. The slightly higher HOMO-LUMO gap for **3b** indicates that the 3-membered ring in the equatorial plane is favouring stabilization.

Conclusions

In this paper, we report the theoretical design of three types of Hp carbon compounds. In type **1** compounds, the delocalization of electron density to empty p-orbitals of boron and σ-donating equatorial lithium atoms stabilizes the compound. The compound **2a** with highest like stabilization effect is observed. For type **3** compounds, the electron-donating ability and the bridging proclivity of lithium are employed along with the inductive stabilization and the negative conjugation like effect of the nitrogen lone pairs. All these molecules computed to have no negative frequencies and the wave functions are stable.

The valence population of carbon obtained by the NBO analysis shows the effective delocalization of electrons on Cp_z orbitals. The sufficient HOMO-LUMO gap assures the stability of the designed compounds. Thus, we have put forward a hybrid way to stabilize tetracoordinate Hp carbon compounds using a suitable combination of axial and equatorial substituents which could hold the carbon atom firmly in its Hp configuration by electronic stabilization. This offers further scope to open up research in designing stable tetracoordinate Hp carbon compounds.

11

Accepted Manuscript

12

References

[1]   U. Radius, S. J. Silverio, R. Hoffmann, R. Gleiter, *Organometallics*. **1996**, 15, 3737-3745.

[2]   J. S. Bradley, G. B. Ansell, M. E. Leonowicz, E. W. Hill, *J. Am. Chem. Soc*. **1981**, 103, 4968-4970.

[3]   S. Harris, J. S. Bradley, *Organometallics*. **1984**, 3, 1086-1093.

[4]   J. S. Bradley, *Adv. Organomet. Chem*. **1983**, 22, 1-58.

[5]   W. J. Evans, T. J. Boyle, J. W. Ziller, *J. Organomet. Chem*. **1993**, 462, 141-148.

[6]   D. L. Clark, J. C. Gordon, J. C. Huffman, J. G. Watkin, B. D. Zwick, *Organometallics*. **1994**, 13, 4266-4270.

[7]   R. E. von H. Spence, D. J. Parks, W. E. Piers, M. A. MacDonald, M. J. Zaworotko, S. J. Rettig, Angew. *Chem. Int. Ed. Engl*. **1995**, 34, 1230-1233.

[8]   K. B. Wiberg, *Chem. Rev*. **1989**, 89, 975-983.

[9]   K. B. Wiberg, J. R. Snoonian, *J. Org. Chem.* **1998**, 63, 1390-1401.

[10]   H. Dodziuk, K. S. Nowinski, *J. Mol. Struct*. **1994**, 311, 97-100.

[11]   R. M. Minyaev, V. I. Minkin, T. N. Gribanova, A.G. Starikov, R. Hoffmann, *J. Org. Chem*. **2003**, 68, 8588-8594.

[12]   K. P. Katin, M. M. Maslov, *Mol. Simulat*. **2018**, 44, 703-707.

[13]   Z. X. Wang, T. K. Manojkumar, C. Wannere, P. V. R. Schleyer, *Org. Lett.* **2001**, 3, 1249-1252.

[14]   A. Streitwieser Jr, C. M. Berke, G. W. Schriver, D. Grier, J. B. Collins, *Tetrahedron.* **1981**, 37, 345-358.

[15]   J. B. Collins, J. D. Dill, E. D. Jemmis, Y. Apeloig, P. V. R. Schleyer,R. Seeger, J.A.Pople, *J. Am. Chem. Soc*. **1976**, 98, 5419-5427.

[16]   J. D. Dill, P. V. R. Schleyer, J. A. Pople, *J. Am. Chem. Soc*. **1976**, 98, 1663-1668.

[17]   T. Clark, G. W. Spitznagel, R. Klose, P. V. R. Schleyer, *J. Am. Chem. Soc*. **1984**, 106, 4412-4419.

[18]   W. Siebert, A. Gunale, *Chem. Soc. Rev*. **1999**, 28, 367-371.

[19]   M. J. Frisch, G. W. Trucks, H. B. Schlegel, G. E. Scuseria, M. A. Robb, J. R. Cheeseman, G. Scalmani, V. Barone, B. Mennucci, G. A. Petersson, H. Nakatsuji, M. Caricato, X. Li, H. P. Hratchian, A. F. Izmaylov, J. Bloino, G. Zheng, J. L. Sonnenberg, M. Hada, M. Ehara, K. Toyota, R. Fukuda, J. Hasegawa, M. Ishida, T. Nakajima, Y. Honda, O. Kitao, H. Nakai, T. Vreven, J. A. Montgomery, Jr., J. E. Peralta, F. Ogliaro, M. Bearpark, J. J. Heyd, E. Brothers, K. N. Kudin, V. N. Staroverov, R. Kobayashi, J. Normand, K. Raghavachari, A. Rendell, J. C. Burant, S. S. Iyengar, J. Tomasi, M. Cossi, N. Rega, J. M. Millam, M. Klene, J. E. Knox, J. B. Cross, V. Bakken, C. Adamo, J. Jaramillo, R. Gomperts, R. E. Stratmann, O. Yazyev, A. J. Austin, R. Cammi, C.

Accepted Manuscript

Pomelli, J. W. Ochterski, R. L. Martin, K. Morokuma, V. G. Zakrzewski, G. A. Voth, P. Salvador, J. J. Dannenberg, S. Dapprich, A. D. Daniels, Ö. Farkas, J. B. Foresman, J. V. Ortiz, J. Cioslowski, D. J. Fox, *Gaussian, Inc. Gaussian 09, Revision A.02, Wallingford CT*, **2009**.

[20]   Y. Pei, Z. C. Zeng, *J. Am. Chem. Soc*. **2008**, 130, 2580-2592.

[21]   https://www.chemcraftprog.com

[22]   F. Weinhold, C. R. Landis, *Chem. Educ. Res. Pract*. **2001**, 2, 91-104.

[23]   F. Weinhold, *J. Comput. Chem*. **2012**, 33, 2363-2379.

[24]   T. Lu, F. Chen, *J. Comput. Chem*. **2012**, 33, 580-592.

[25]   https://www.ks.uiuc.edu/Research/vmd

[26]   D. Röttger, G. Erker, Angew. *Chem. Int. Ed. Engl*. **1997**, 36, 812-827.

[27]   R. Hoffmann, R. W. Alder, C. F. Wilcox Jr, *J. Am. Chem. Soc.* **1970**, 92, 4992-4993.

[28]   T. L. Brown, J. A. Ladd, G. N. Newman, *J. Organomet. Chem.* **1965**, 3, 1-6.

[29]   R. M. Minyaev, V. I. Minkin, Russ. *J. Gen. Chem*. **2008**, *78*, 732-749.

[30]   R. Keese, *Chem. Rev*. **2006**, 106, 4787-4808.

[31]   L. M. Yang, E. Ganz, Z. Chen, Z. X. Wang, P. V. R. Schleyer, Angew. *Chem. Int. Ed.* **2015**, 54, 9468-9501.

[32]   M. P. McGrath, L. Radom, H. F. Schaefer III, *J. Org. Chem*. **1992**, 57, 4847-4850.

[33]   K. Sorger, P. von Ragué, *J. Mol.Struc.(Theochem).* **1995**, 338, 317-346.

[34]   E. Lewars, *J. Mol. Struc. (Theochem).* **1998**, 423, 173-188.

[35]   E. Lewars, J. *Mol. Struc. (Theochem)*. **2000**, 507, 165-184.

[36]   J. P. Kenny, K. M. Krueger, J. C. Rienstra-Kiracofe, H. F. Schaefer, *J. Phys. Chem. A*. **2001**, 105, 7745-7750.

[37]   V. I. Minkin, R. M. Minyaev, *Dokl. Chem*. **2002**, 385, 203-206.

[38]   E. G. Lewars, Modeling Marvels: Computational Anticipation of Novel Molecules, Springer, Amsterdam, **2008**.

[39]   R. M. Minyaev, T. N. Gribanova, V. I. Minkin, A. G. Starikov, R. Hoffmann, *J. Org. Chem*. **2005**, 70, 6693-6704.

[40]   W. L. Jorgensen, W. T. Borden, *J. Am. Chem. Soc.* **1973**, 95, 6649-6654.

[41]   A. Rauk, Orbital Interaction Theory of Organic Chemistry, 2nd Edn, John Wiley & Sons, New York, **2001**, 34-85.